Biosorption of Heavy Metal Ions Using Green Algae (Sargassum Wightii) – Equilibrium, Kinetics and Thermodynamic Studies

Yogeshwaran, Venkatraman*+

Department of Civil Engineering, Sri Krishna College of Engineering and Technology, Coimbatore, INDIA

Priya, Arunkumar

Department of Chemical Engineering, KPR Institute of Engineering and Technology, Coimbatore, INDIA

ABSTRACT: *The removal of heavy metal ions (Cr, Pb, and Zn) present in aqueous solutions has been examined using Sargassum Wight (SW) - brown algae – as an organic adsorbent. The functional groups of SW were determined by FT-IR analysis before and after heavy metal ion adsorption. Because of the strong Van der Walls forces, the SEM/EDX picture reveals the presence of heavy metal ions on the surface of the SW. The influence of adsorption was studied in different settings by adjusting the parameters of pH, SW dosage, metal ion concentration, time of contact, and temperature. In addition, thermodynamic and isotherm investigations were carried out in order to determine the adsorption process and its connection. It was found that by adding 0.3 N H_2SO_4, the maximal desorption rate was achieved. Around 99.6% of chromium ions, 89.27% of lead ions, and 82.39% of zinc ions were removed from the synthetic solutions through batch-mode adsorption studies.*

KEYWORDS: *Heavy metals, Adsorption, Sargassum Wightii, Thermodynamic studies, Kinetic studies.*

INTRODUCTION

Water contamination is one of the most important concerns that the world has been dealing with for ages. Owing to free industrial and agricultural activities, coupled with human ignorance in terms of the unplanned disposal of wastes, water bodies around the globe have witnessed much-increased levels of contamination in recent days. Changes in the water's physical and chemical qualities that result from contamination render the water unfit for drinking. Colours, heavy metals, organic pollutants (suspended or dissolved), and other contaminants often pollute water in exceedingly high quantities [1]. Particularly, heavy metal pollution of water is one of the most significant issues because of the toxicity of metal ions, which becomes extremely damaging to the environment and humans at high concentrations of contamination [2]. With the rise of heavy metal pollution, the globe now confronts many health concerns, including cancer, lung disorders, and other ailments. As a result, before discharging wastewater into the environment, it is critical to diminish or eliminate the presence of heavy metal ions in the wastewater [3]. To date, several studies have been performed to reduce the build-up of heavy metal

* *To whom correspondence should be addressed.*
+ *E-mail: svyogi23190@gmail.com*
1021-9986/2023/11/3624-3639 16/$/6.06

Table 1: Adsorption of various heavy metals using algae-based biomass products

S. No.	Type of pollutant (s)	Type of Algal species	Metal ion uptake	Initial metal ion conc.	Ideal pH	adsorbent dose	Time of contact	Ref.
1.	Cr, Pb & Zn	Sargassum Wightii – Brown Algae	99.6%, 89.27% & 82.39%	25 mg/L	2.0	2.0 g/L	60 min	this study
2.	Cu, Zn & Ni	brown macro-algae	92%	50 mg/L	3.0	1.0 g/L	200 min	[12]
3.	As, B, Cu, Mn & Zn	Green micro – algae	30.9%, 22%, 85.2%, 66.1 & 95.9%	12 mg/L, 60 mg/L, 3 mg/L, 3 mg/L & 3 mg/L	5.5, 7.0 & 9.0	0.025 mg/L	3 h & 10 min	[13]
4.	Hg	Chlorella vulgaris – Green micro algae	17.32 mg/g	77.9 mg/L	5.0	2.0 g/L	90 min	[14]
5.	Cd	Nannochloropsis oculate – Single cell algae	232.55 mg/g	1000 mg/L	5.0	0.392 g /50 mL	60 min	[15]

ions in wastewater using different techniques and methodologies. The adsorption method has focused on eliminating metal ion concentration by utilizing batch and fixed bed processes to build a unique treatment procedure that responds to an urgent demand [4]. This method offers a few benefits, including minimal capital costs, selective metal removal, and desorption without sludge production. Using the adsorbate, the pollutants present in the aqueous medium have been removed by the adsorption process through batch and column studies [5]. Both natural and industrial by-products (decomposable) were used in many research studies to reduce pollutant concentrations. To improve the efficacy of the adsorption process, the adsorbent material is usually transformed into activated carbon [6].

Organically decomposable materials such as fruit seeds and peels, tree bark and leaves, industrial wastes of fly ash, and blast furnace slag have been used as biosorbent materials to remove the many toxic metal ions from aqueous media. Apart from the materials, many bacteria, algae, etc., have been used as bio-adsorbents for reducing the toxic pollutants in the aqueous solutions [7]. Using organic material and industrial by-products as adsorbent material, which results in secondary pollutant generation, and desorption of pollutants from the adsorbent material are challenging tasks [8]. On the other hand, by using biological materials and other organic matter, many toxic metals have been removed from polluted sources without the formation of secondary pollutants, and removing the accumulated pollutant from the adsorbent has been done in many easy ways [9]. Within the domain of microorganisms, algae, which involve photosynthesis for their growth, are available in marine and fresh waters [10]. Due to their food and fuel production abilities, algae are considered fast-growing beings; and they possess the ability to produce biomass from nutrients using atmospheric CO_2 [11]. In this experimental work, Sargassum Wigtii's role in removing toxic metal ions (Cr, Pb, and Zn) and its importance has been discussed. Table 1 represents the comparison study of various heavy metal ions and their adsorption using different types of algae.

The main objective of this experimental study is to check the adsorption behaviour of chemically prepared biosorbents of SW brown algae for metal ion removal in batch mode and to check the performance of adsorption by various kinetic and isotherm studies. The spent adsorbent material was regenerated and used several times in batch adsorption studies using the desorption process. The three- and four-parameter isotherm studies of the Temkin, D-R, and Sips models were studied to check the actual performance of the adsorption process. Also, Boyd kinetic studies were conducted to check the rate-controlling step of the adsorption process due to external and internal film diffusion.

EXPERIMENTAL SECTION

Preparation of adsorbent and Stock solution

The brown algae adsorbent, SW, was collected from Nagapattinam district, Tamil Nadu, India, and was washed several times to remove the impurities by using double distilled water. Then the collected SW was dried in sunlight for 10 days, cut into small pieces, and crushed several times with a domestic mixer (1 HP Micro Active, India) to obtain a range of particle sizes between 150 and 175 µm for porous material preparation. The crushed SW was then kept in an oven at 60°C for 24 hours to further remove impurities. The chemicals potassium dichromate ($K_2Cr_2O_7$), zinc chloride ($ZnCl_2$), and lead sulphate ($PbSO_4$) were procured from Precision Scientific Co. Ltd., Coimbatore, with a purity of 99.5%. For the stock solution preparation, 50 mg of $K_2Cr_2O_7$, $ZnCl_2$, and $PbSO_4$ were taken and mixed with 500 mL of double-distilled water,

and the solution was kept at room temperature. The double distilled water dilution was done to obtain the designed concentrations at various levels. The pH of the solution was adjusted by adding 0.1 M of H_2SO_4.

Pore distribution & BET surface area

The adsorption-desorption isotherm process was used to obtain the diameter of the pore and its size distribution, BET surface area, and other micro- and mesopores of SW using nitrogen at -196°C for this porous material. The vacuum area of SWs adsorbent material was found by keeping the adsorbent at 300°C for 5 hours to remove gas molecules. Using the Dubinin-Radushkevich (D-R) process, the relationship between micro and meso pores was obtained by referring to Eq. (1).

$$S_m = S_{BET} - S_u \quad (1)$$

Were, S_m – average micro pore size of sewage sludge, S_u – average meso pore size of sewage sludge, S_{BET} – average surface area found in BET analysis

the relative pressure of P/Po~0.99, the pore Under volume (V_T), and the amount of nitrogen required for BET analysis were obtained. The amount of meso and micropores in the SWs adsorbent was calculated using Eq. (2).

$$V_m = V_T - V_u \quad (2)$$

Also, the pore diameter (D_P) was calculated using the Eq. (3).

$$D_P = \frac{4\,V_T}{S_{BET}} \quad (3)$$

Batch Adsorption Studies

By varying the parameters of metal ion contact time with SW, amount of SW used initial concentration of metal ions, potential of hydrogen (pH), and temperature, batch adsorption experiments were performed. Within the equilibrium period (60 min), the impact of varying adsorption parameters, such as concentration of Cr, Pb, and Zn metal ions (50 mg/L with 100 mL of aqueous solution) and pH (2.0 to 7.0), on SW's dosage (0.5–2.5 g/L) was determined at a constant temperature of 30°C. To attain equilibrium, the samples with the SW were kept in a rotary shaker and shaken for 60 minutes, and the particles were allowed to settle for up to 15 minutes. The contact time between the heavy metal ions and SW was adjusted from 10 minutes to 2 hours. The amount of metal ions adsorbed by the SW adsorbent was obtained by using Eq. (4) at different time intervals.

$$q_t = \frac{(C_o - C_t)\,V}{m}\ \text{mg/g} \quad (4)$$

q_t – Total amount of adsorbed metal ions by SW (mg/g), C_t – Batch adsorption process and its concentration, V – Volume of the solution, m – Mass of the adsorbent

The residuals were then collected from the conical flask and analyzed by Atomic Adsorption Spectroscopy (AAS) to determine the percentage of metal ions (Cr, Pb & Zn) adsorbed by SW. Each analysis was repeated twice to obtain the concurrent value, and the average value was taken. Eq. (5) provides the percentage of adsorbed metal ions by SW.

$$\%\ \text{Removal} = \left[\frac{C_o - C_e}{C_o}\right] X100 \quad (5)$$

C_o & C_e – Initial and Equilibrium concentration of the solution, V – Solution's volume, m – Adsorbent mass

Kinetic Studies

By varying the heavy metal ions and their concentrations (25–150 mg/L), the equilibrium studies were carried out at a pH level of 2.0 and 2 g/L of SW in a 100 mL solution. The solution was subjected to a rotary shaker for 60 minutes at 120 rpm speed at 30°C, followed by filtration using Whatman filter paper. The following adsorption active models were utilized to examine the obtained data concerning the adsorption proficiency and the achievability of the scale-up tasks.

Pseudo – First order kinetic model

Based on solid adsorption capacity, this model, also known as the Lagergren kinetic rate model, was developed for the adsorption of solid and liquid systems [16]. This represents the researchers' sole kinetic model for solute adsorption from a liquid solution. According to the author's conclusion, the driving force is exactly proportional to the total adsorption rate, i.e., the difference between the initial and equilibrium adsorbate concentrations ($q_e - q$). Eq. (6) was used to express the pseudo-first-order kinetic model:

$$\frac{dq_e}{dq_t} = k\,(q_e - q_t) \quad (6)$$

At the equilibrium, the total amount of metal ions adsorbed at time (t) was obtained by calculating q_e & q_t, where K is the rate constant. Using the boundary layer conditions, the Eq. (4) can be rearranged as Eq. (7).

$$\log(q_e - q) = log q_e - \frac{k}{2.303}t \quad (7)$$

Pseudo – second-order kinetic model

This kinetic analysis uses the second-order chemical adsorption process, with the assumption that the rate of adsorption is proportional to the square of the number of empty sites [17]. Eq. (8) expresses the pseudo second-order kinetic Equation.

$$\frac{d_q}{d_t} = k(q_e - q)^2 \quad (8)$$

By applying boundary conditions (t = 0 to t > 0, and q = 0 to q > 0), the Eq. (8) can be rearranged as Eq. (9).

$$\frac{t}{q} = \frac{1}{h} + \frac{1}{q_e}\, t \quad (9)$$

where, h = kq_e^2 – Initial adsorption rate, and k – rate constant. A plot of t/q_t vs. time at various adsorption parameters provides a linear relationship, allowing the determination of 'q_e', 'k' and 'h'.

Boyd kinetic model

The information found in the Boyd kinetic plot was utilized to analyze the slowest step of the adsorption process by the adsorbent [18]. The Boyd kinetic Equation is presented as Eq. (10).

$$\frac{q_t}{q_e} = 1 - \frac{6}{\Pi^2}\exp(-Bt) = F \quad (10)$$

q_t & q_e – Total quantity of heavy metal ions adsorbed at time 't' in the equilibrium (mg/g), F – Fraction of metals adsorbed at any time 't', B – Mathematical function, taking natural logarithm in Eq. (7), it can be rearranged as Eq. (11).

$$Bt = -0.4977 - \ln(1 - F) \quad (11)$$

To access the linearity of experimental data, the plot (B_t vs. t) was used. The B_t values were used to calculate the effective diffusion coefficient, D_i (m^2/s), using the Eq. (12).

$$B = \frac{\Pi^2 D_i}{r^2} \quad (12)$$

The effective diffusion coefficient (D_i) and the radius of the adsorbent (r) were found using Eq. (12). Moreover, based on the assumptions in sieve analysis, the radius of the adsorbent particles was calculated.

Isotherm studies

Adsorption isotherms provide better knowledge of the connection between the adsorbate and the adsorbent, which is vital for optimal adsorbent use. To optimize the adsorption mechanism, accurate inferences must be drawn from the equilibrium plot [19]. The adsorption isotherm created as a result gives critical data for assessing production in a large-scale industrial system.

Temkin isotherm study

According to this adsorption isotherm, the adsorption strength of all molecules in the layer decreases linearly with distance due to indirect adsorbate / adsorbent contact [20]. Eq. (13) expresses the isotherm Equation derived from Temkin studies.

$$q_{eq} = \frac{RT}{b}\ln K_T + \frac{RT}{b}\ln C_e \quad (13)$$

The binding constant at the equilibrium (K_T), temperature (T), universal gas constant (R), and adsorption heat constant (b) were used to find out the adsorbate equilibrium concentration (C_{eq}) by Temkin isotherm studies.

D-R isotherm study

The homogeneity or potential sorption of the adsorption process is not assumed, and the D-R (Dubinin–Radushkevich) Equation is more analogous compared to other isotherm studies. Eq. (14) expresses the D-R character of the adsorption process Equation.

$$\ln q_e = \ln x_m - \beta €^2 \quad (14)$$

q_e – Quantity of metal ions adsorbed in the equilibrium time, x_m – Capacity of the adsorption in mg/g

Sips isotherm study

The Langmuir & Freundlich isotherm models were combined to predict the process of adsorption in the heterogeneous sips isotherm system. The sips model forecasts monolayer adsorption when the concentration of the solution is very high. Also, the solution's attention is completely avoided and follows the Langmuir model. The expression for the sips isotherm model can be expressed in Eq. (15).

$$\frac{1}{q_e} = \frac{1}{Q_{max}K_s}\left(\frac{1}{C_e}\right)^{\frac{1}{n}} + \frac{1}{Q_{max}} \quad (15)$$

Q_{max} and K_s – Adsorption capacity and equilibrium constant obtained from the slope and intercept in linear plots and n - factor of heterogeneity lies between 0 to 1.

RESULTS AND DISCUSSION

SEM/EDX Analysis

The surface of SW before and after the adsorption of heavy metal ions (Cr, Pb, and Zn) is shown in Figs. 1 (a) and (b). The presence of uneven holes on the surface of the adsorbent was observed, and this was due to the sulfuric acid

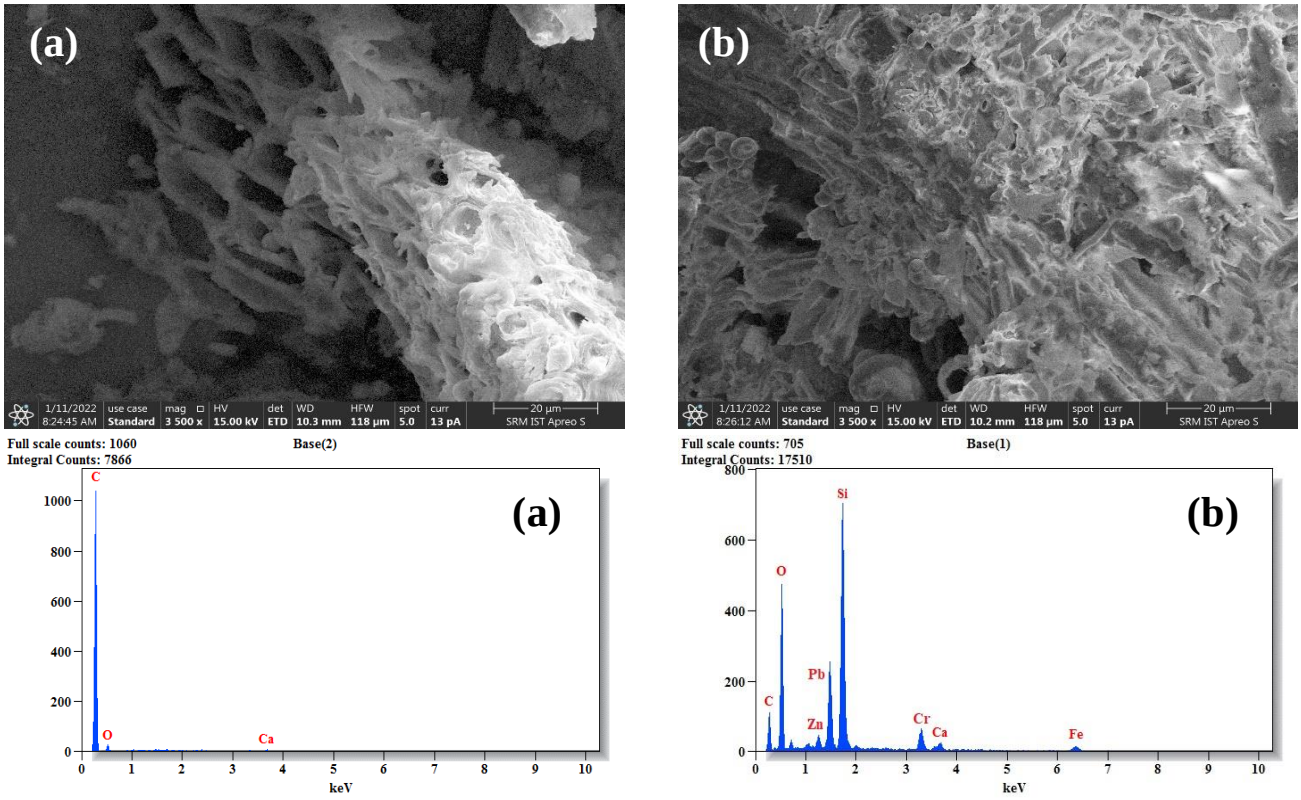

Fig. 1: (a) & (b) – SEM & EDX images of raw and metal ions adsorbed SW.

treatment that saturated the porous material surfaces on the adsorbent. Referring to the SEM image of the adsorbent material, before passing the metal ion-containing solution, there were uneven pores and vacant sites. When the metal ion-containing solution was passed and stayed up to a saturation period, the pores were filled with pollutants, and no vacant sites were identified. Hence, it confirms the adsorption process on the adsorbent material. To confirm the presence of targeted pollutants, EDX analyses were performed. The EDX image shows the presence of Cr, Pb, and Zn metal ions after the adsorption process, along with other metal elements and components such as chlorine, nicotine, and sulfur. During the acid treatment, the SW powder reacted with sulfuric acid, and the hydroxyl group produced the esters as a non-ionic functional group that may be complex with cations [21]. Also, the roughness of the adsorbent surface was reduced because of the addition of acid, which increased the pores on the adsorbent's surface. Hence, the charged sites got protonated during the acid treatment, and the acid did not destroy the functional groups of the adsorbent.

BET Surface area analysis

The adsorption and desorption isotherm curve shown

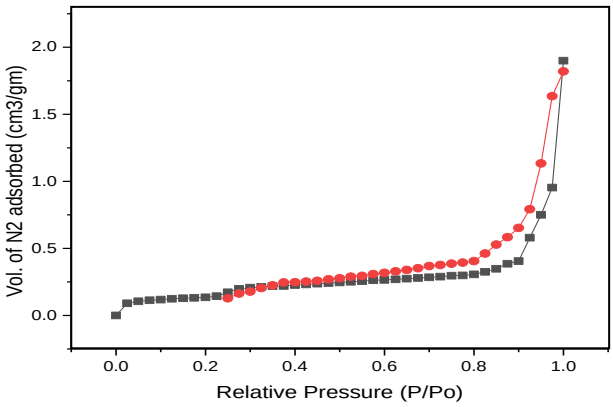

Fig. 2: Adsorption – Desorption Isotherm (Nitrogen).

in Fig. 2 represents the nitrogen desorption rate of SWs biochar adsorbent at -196°C. The rate of adsorption and desorption with nitrogen has been shown in Fig. 2, and the observed characteristics are represented in Table 2. It was realized that the SW possessed micro and meso pores (Type II) and a BET surface area of around 654 m^2/g, which is more than the pore volume (0.412 cm^3/g) of other commercial activated carbons [22]. The sewage sludge adsorbent material has 310 m^2/g surface area [23], and coal-derived biomass material has 1826.41 m^2/g surface

Table 2: Pore characteristics of SW adsorbent

S. No.	Parameter	Units	Value
1.	BET surface area	m^2/g	654
2.	Pore volume	cm^3/g	0.412
3.	Micro pore volume	cm^3/g	0.189
4.	Meso pore volume	cm^3/g	0.082
5.	Micro pore area	m^2/g	392
6.	Average pore diameter	Nm	0.6 – 2.4

area [24], both of which have been reported in many research works that confirm the range of surface area of prepared biosorbent materials.

FT-IR – Studies

Fig. 3 shows the various functional groups of raw SW and metal ions-loaded SW separately. The O-H stretching vibrations were noticed as the band at 3392 cm^{-1}, which can be attributed to the presence of amide and water groups. The peak at 2922 cm^{-1} belongs to the -CH_3 group. The production of N-H was realized from the stretching vibration of C=O at 1693 cm^{-1}. The band's bending vibrations represent CH_3 groups at about 1098 cm^{-1}. The -OH stretching frequencies were observed to shift from 3352 cm^{-1} to lower frequencies, which is demonstrated by the metal ion-loaded spectrum. Similarly, the –CH_3 group's stretching and twisting vibrations moved to a lower frequency. This demonstrates metal ion binding onto the binding sites of SW [25].

Effect of pH on metals adsorption

Adsorption tests were carried out at various pH levels (2.0 to 7.0). Fig. 4 shows that when the pH of the solution increased from 2.0 to 7.0, the quantity of metal ion adsorption dropped from 99.6 to 64.4% for Cr, 94.43 to 75.21% for Pb, and 91.2 to 82.63% for Zn. Due to the properties of protonation, metal ion adsorption was increased at lower pH values. When the hydrogen ion concentration is high (at a lower pH), the negative charge of the internal pore surface is neutralized, and there arises the possibility of the development of new adsorption sites with positive charges that adsorbed the anionic complexes (Cr, Pb, and Zn) on the surface [26]. Furthermore, the starting pH of the solution was always lower than the final pH. This supports the neutralization of negatively charged ions drawn to the surface by the H^+ ions and the production of additional H^+ ions in the positively charged surface [27].

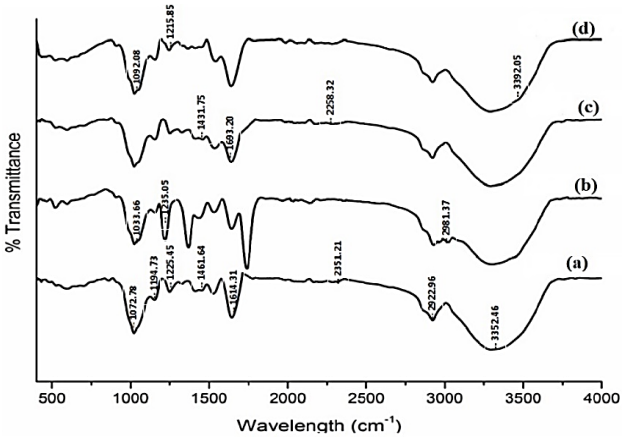

Fig. 3: FT-IR image of (a) Raw and (b), (c) & (d) metal ions (Cr, Pb & Zn) loaded SW.

As a result, the pH of the solution increased while the concentration of H+ ions in the solution decreased. Based on the above discussion, it was found that the maximum amount of efficiency was attained at an optimum pH of 2.0.

pH - Zero Point Change (pH_{ZPC})

Referring to Fig. 4, 35.42% of chromium ions were removed by changing the pH of the metal ion-containing solution from 2.0 to 7.0. This scenario was improved with a further increase in pH, which resulted in the conversion of chromium ions from hexavalent to trivalent. Eqs. (16) and (17) show the variations and conversion of chromium ions from a hexavalent state to a trivalent state. Due to the adsorbent material's protonation property, adsorption efficiency was increased at lower pH levels. Also, high amounts of hydrogen ions and their concentrations at lower pH can react with the negatively charged ions on the adsorbent's surface. Hence, the negatively charged ions were neutralized, and new active sites were developed with positive charges of metal ion complexes. Furthermore, the metal ion-containing solution's initial pH was lower than the metal ion solution's final pH. It neutralized the H+ ions with negatively charged ions on the surface and developed a high amount of H+ ions with positive charges. This trend was also seen in Fig. 4 for Pb (II) and Zn (II) ions.

$$Cr_2O_7^- + 14\,H^+ + 6e^- = 2Cr^{3+} + 7H_2O \quad (16)$$

$$HC_rO_4^- + 7H^+ + 3e^- = Cr^{3+} + 4H_2O \quad (17)$$

During the lower pH conditions, a higher efficiency rate could occur based on the chemical characteristics of SW's biochar surface. When the pH of the chromium ion

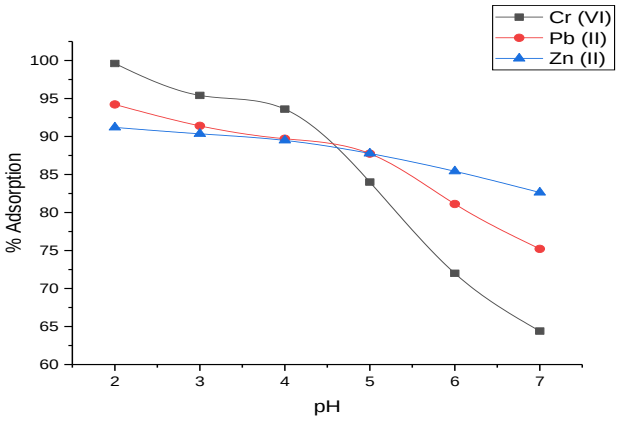

Fig. 4: Changes in metal ion adsorption by varying the pH.

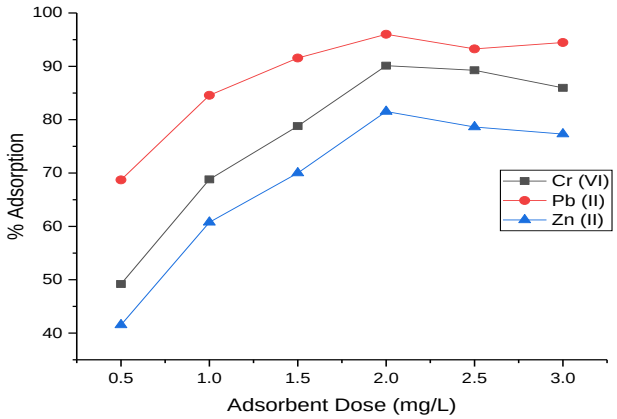

Fig. 5: Changes in metal ion adsorption by varying the SW's dose.

solution is in an acidic state, the formation of chromium ions is $Cr_2O^-_7$ and $HCrO^-_4$, which produce a very high adsorption rate. But the chromium ion solution is in the alkalinity range. Cr^{6+} ions were completely destroyed, which reduced the adsorption rate. When the pH is very low, a large amount of H^+ ions neutralize the negatively charged sites and reduces the interference of dichromate ions. Also, the adsorption capacity of Pb^{2+} ions was decreased when the pH of the metal ion solution was within the range of 4.0 to 7.0. Due to the rivalry between Pb ions and OH^- ions, the adsorption capacity decreased and the H^+ ion concentrations increased. A similar trend was followed for Zn^{2+} metal ions when the solution pH was within 4.0 to 7.0. The hydronium (H_3O^+) ions were produced at lower pH values and associated with the SW surface to maintain the net positive charge.

Effect of SW concentration on metals adsorption

Fig. 5 depicts the effect of SW's dosage on the adsorption of Cr, Pb, and Zn metal ions. At an SW dosage

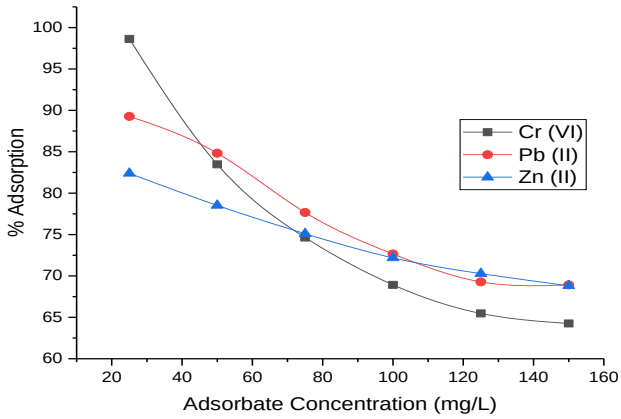

Fig. 6: Changes in metal ion adsorption by varying the metal ion concentrations.

of 1 g/L, the maximum percentage removal of metal ions was determined to be 90.12% for Cr, 96.01% for Pb, and 81.53% for Zn, and it was found to stay practically constant after that. This occurrence may be attributed to a decrease in the aqueous solution's concentration gradient. The increase in percentage adsorption with increasing adsorbent dosage may be attributed to an increase in free surface accessibility, which produced an increase in adsorbate molecules [28]. The optimal SWs dosage was determined to be 1 g/L and was used in the subsequent experiments.

Effect of solution concentration on metal ions adsorption

Initially, the adsorption tests were conducted by fixing the metal ion concentration at 25 mg/L, followed by an increase up to 150 mg/L. Fig. 6 shows the gradual decrement in adsorption efficiency when the concentration of metal ions is increased. The amount of metal ion adsorption was increased from 64.26 to 98.63 % for Cr, 68.92 to 89.27 % for Pb, and 68.82 to 82.39 % for Zn, with a decrease in the primary concentrations of the heavy metal ions. The percentage removal efficiency was found to rise consistently when the adsorbate concentration was decreased, showing that the adsorbent material did not achieve saturation [29].

Effect of contact time on metals adsorption

The contact time between the SW adsorbent and heavy metal ions was adjusted from 10 min to 2 hrs., and the effects were studied and represented in Fig. 7. During the initial stages, the metal ion elimination was highly rapid, while there were no significant changes at later stages. After 60 minutes, the metal ion uptake reached the constant rate, and there was no improvement in Cr, Pb and Zn metal

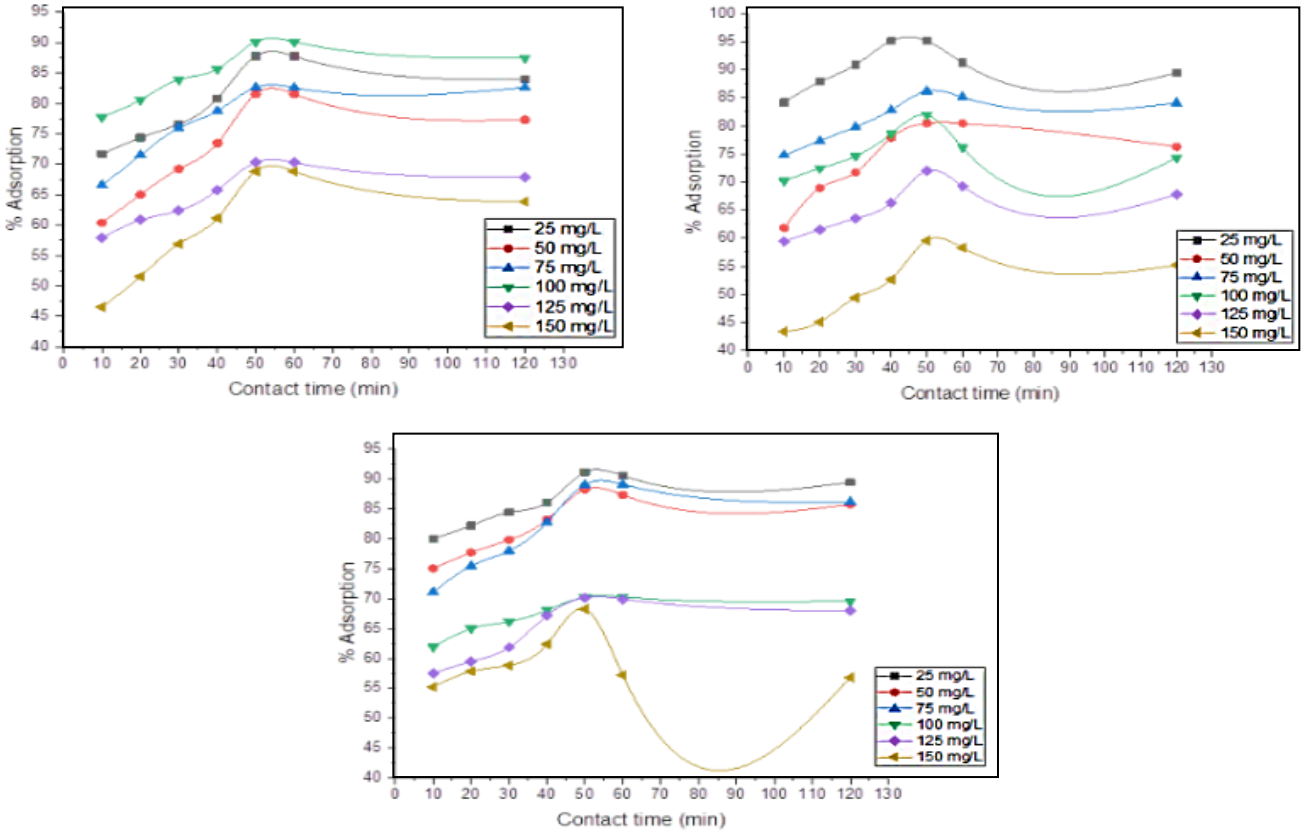

Fig. 7: Changes in metal ion adsorption by varying the contact time.

adsorption. This was because the adsorbate molecules faced saturation of their solid surfaces, leading to a decrease in the metal ion uptake after 60 min due to repulsive forces [30]. Also, the passage of time resulted in a decrease in mass transfer between the solid and liquid phases, as the heavy metal ions need to travel very long distances through the pores with very high concentrations [31].

Effect of temperature on metals adsorption

Taking the concentration of heavy metal ions as 50 mg/L with 2.5 g/L of SW's concentration, the temperature impact was analyzed for up to 60 minutes. Initially, the percentage of adsorption rose to 30°C before gradually decreasing. As a result, optimal adsorption occurred at 30°C. The drop in percentage adsorption at 45°C might be attributed to a rise in the desorption rate [32]. Fig. 8 shows the adsorption effectiveness of the adsorbents at various temperatures ranging from 15 to 60 °C.

Pseudo – First order kinetic study

The kinetic plot of log (q_e - q) vs. time (t) for heavy metal ion (Cr, Pb, and Zn) adsorption is shown in Fig. 9,

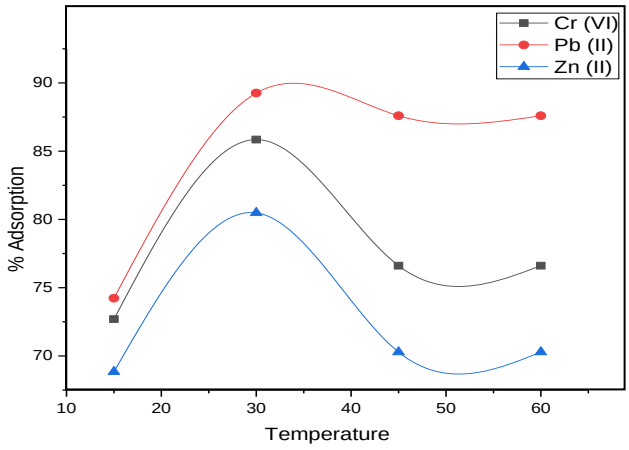

Fig. 8: Changes in metal ion adsorption by varying the temperature.

obtained using Eq. (5). Based on the linearity of the plots, the rate constant and the correlation coefficient (k and R^2, respectively) were calculated and presented in Table 3. The R^2 values were found to be low (< 0.95), and this model does not fit with the pseudo-first-order kinetics, which indicates that the adsorption process has not reached equilibrium status [33]. By referring to the linear plots of this study, the amount of metal ion uptake by biochar

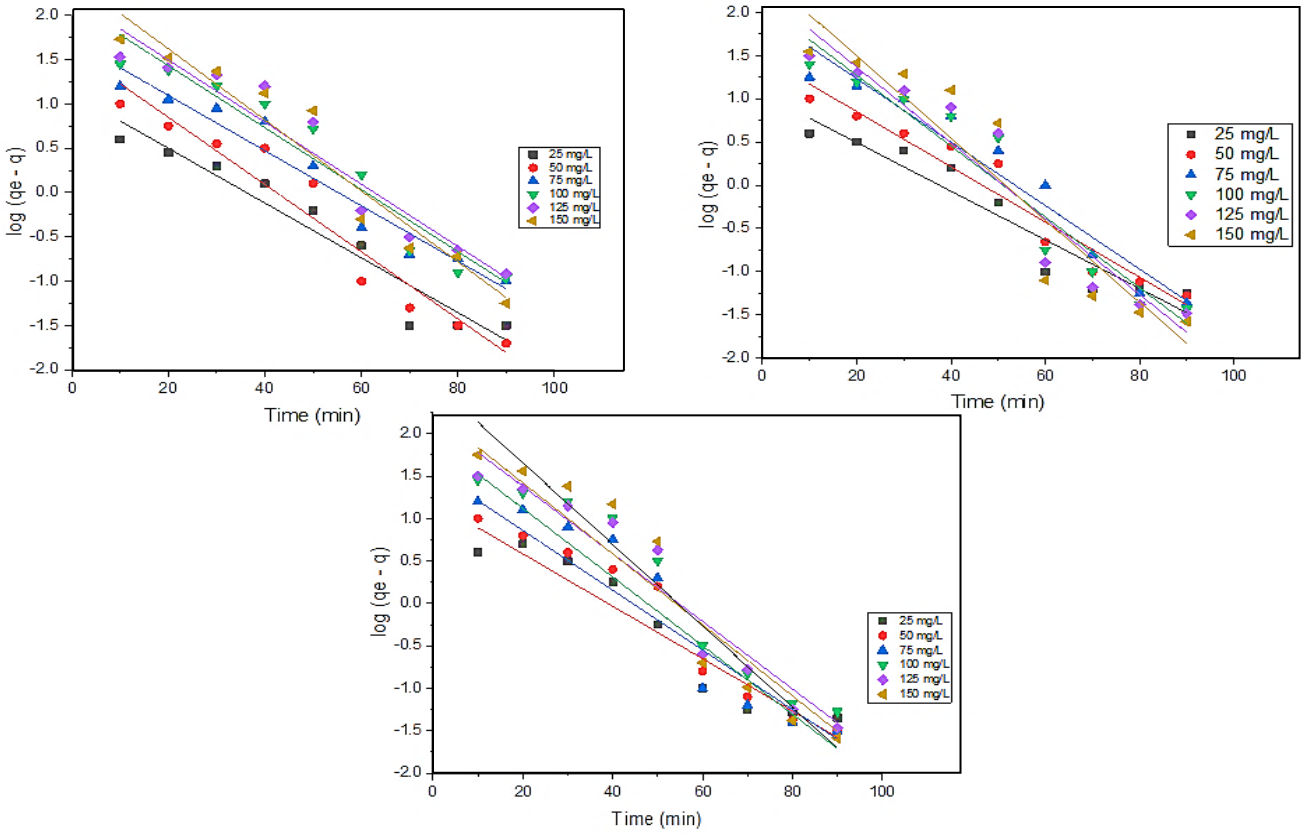

Fig. 9: Pseudo-first-order kinetic plot for heavy metal (Cr, Pb and Zn) removal using SW.

adsorbent was not linearly fitted with the amount of adsorbent solute released from the adsorbent. Hence, the process of metal ion uptake by the biochar adsorbent was not of a physical nature.

Kinetic studies

Pseudo – Second order kinetic study

Varying the concentrations of metal ions (25–150 mg/L), the second-order kinetic plots (t/q vs. t) were obtained and shown in Fig. 10. Based on the plots and their linearity, the coefficients of correlation (h and k) were calculated and presented in Table 3. From the table, it can be readily realized that both the calculated and the experimental values of qe are nearly correlated, and the R^2 values were > 0.95, which confirms the suitability of this kinetic model as the adsorption process has reached its equilibrium conditions. Also, the process of adsorption was fitted with this second-order study, which confirms that the mechanism of metal ion adsorption through the biosorbent follows a chemical nature. Hence, it is necessary to determine the rate-controlling process of the adsorption process because of the chemical nature of metal ion uptake by the adsorbent.

Boyd kinetic study

The Boyd kinetic plots were used to determine the rate-determining step of the adsorption process. The 'B_t vs. t' plot was used to determine if the experimental variables were linear. Referring to Boyd's kinetic plots (Fig. 11) for chromium, lead, and zinc ion adsorptions by SW, the lines were linear; however, they did pass through the origin point. This is because the external film diffusion of the adsorption of metal ions by SW indicates the film diffusion of metal ion adsorption by SW [34]. Using Fig. 11, the Boyd kinetic parameters (Di & B) were calculated and presented in Table 3, which demonstrated very high regression values (R^2 > 0.95).

Based on the kinetic studies, the metal ion uptake through the SW biosorption followed the chemical nature of the adsorption process with external film diffusion.

Isotherm studies

Temkin adsorption isotherm

The bio-adsorbent (SWs) provided a very high rate of metal ions adsorption from the aqueous solutions. Parameters, such as size and volume of the pore, specific

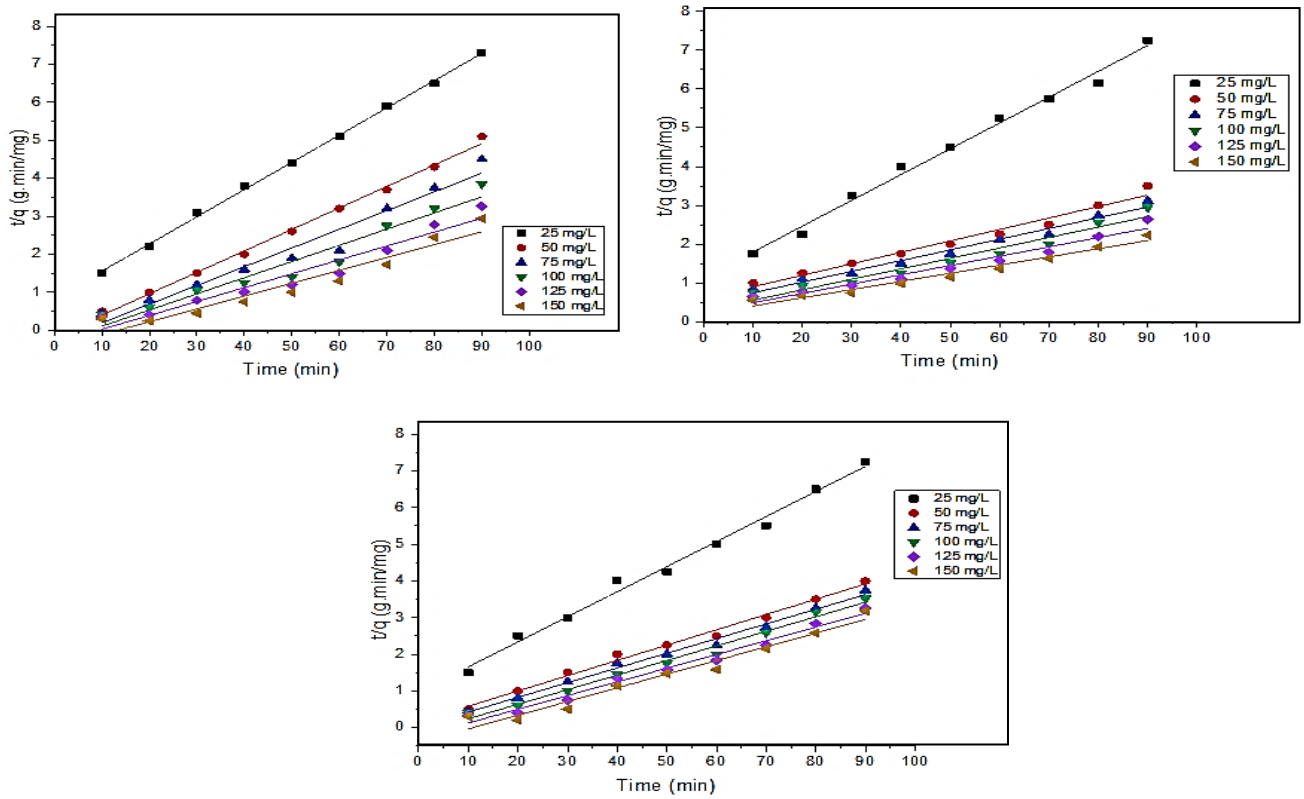

Fig. 10: Pseudo second order kinetic plot for heavy metal (Cr, Pb and Zn) removal using SW.

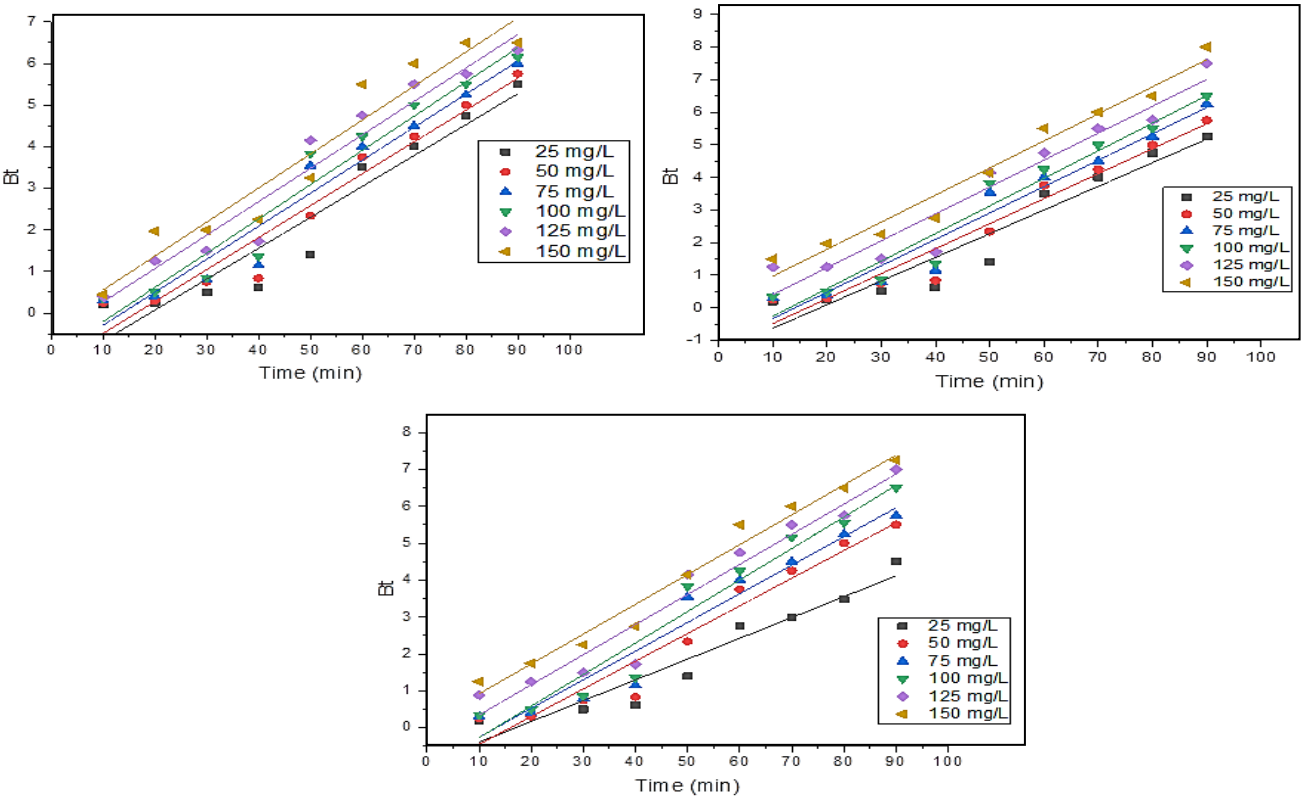

Fig. 11: Boyd kinetic plot for heavy metals (Cr, Pb and Zn) adsorption using SW.

Table 3: Kinetic constants of metal ion adsorption process using SW biochar adsorbent.

S. No.	Nature of the metal ion	Concentration of the ion solution (mg/L)	Pseudo First order			Pseudo Second order					Boyd		
			k (min^{-1})	q_e, cal (mg/g)	R^2	K (g/mg.min) X 10^{-3}	q_e, cal (mg/g)	h (mg/g.min)	q_e, exp (mg/g)	R^2	B	D_i (x $10^{-3}m^2/s$)	R^2
1.	Cr (VI)	25	0.0668	11.492	0.918	8.980	13.988	1.751	12.983	0.997	0.086	11.942	0.918
2.		50	0.0736	28.504	0.921	4.722	26.878	3.607	25.126	0.997	0.074	12.605	0.912
3.		75	0.0760	46.559	0.927	2.826	41.766	3.986	38.214	0.996	0.076	12.848	0.928
4.		100	0.0829	83.716	0.946	1.969	56.552	4.552	50.873	0.995	0.083	14.207	0.944
5.		125	0.0714	84.139	0.936	1.353	66.763	4.793	59.129	0.994	0.085	14.762	0.938
6.		150	0.0692	84.725	0.927	1.114	72.361	5.216	68.427	0.994	0.072	12.974	0.926
1.	Pb (II)	25	0.0678	12.445	0.927	7.763	13.968	1.522	12.840	0.997	0.068	11.492	0.928
2.		50	0.0714	29.040	0.911	3.600	26.513	2.778	24.450	0.997	0.072	12.373	0.914
3.		75	0.0737	54.935	0.928	2.870	38.642	3.623	36.892	0.979	0.086	14.354	0.925
4.		100	0.0875	84.121	0.924	1.530	51.235	4.617	48.711	0.969	0.088	14.730	0.927
5.		125	0.0921	94.189	0.931	0.949	62.458	4.655	59.122	0.994	0.093	15.177	0.931
6.		150	0.0985	132.573	0.943	0.782	72.357	4.925	68.458	0.994	0.096	15.673	0.918
1.	Zn (II)	25	0.0645	11.561	0.916	8.186	13.514	1.495	12.631	0.975	0.066	10.895	0.912
2.		50	0.0737	30.794	0.922	4.250	25.641	2.466	24.221	0.976	0.072	12.605	0.922
3.		75	0.0898	69.343	0.935	2.522	37.307	3.640	35.015	0.964	0.090	15.120	0.936
4.		100	0.0806	74.989	0.930	1.478	52.363	4.908	47,234	0.965	0.083	14.782	0.930
5.		125	0.0875	92.336	0.935	1.258	66.672	5.392	59.286	0.972	0.088	13.520	0.935
6.		150	0.0936	115.88	0.942	1.009	73.314	4.484	67.194	0.964	0.094	12.834	0.918

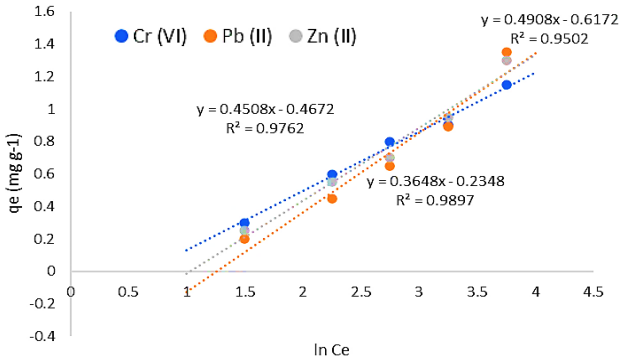

Fig. 12: Temkin plot for the adsorption of heavy metals (Cr, Pb, and Zn) using SW

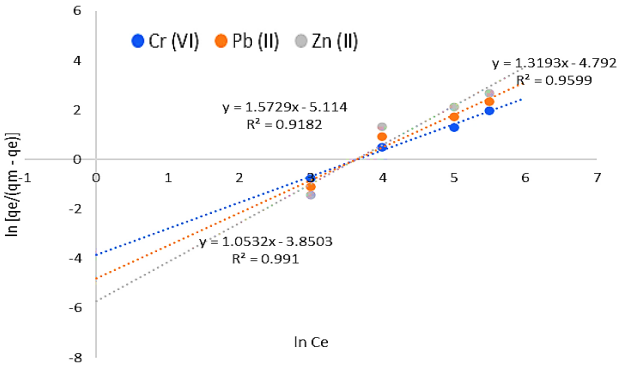

Fig. 13: Sips plot for the adsorption for heavy metals (Cr, Pb and Zn) using SW.

surface area, etc., were obtained using the adsorption isotherm studies. The adsorption process by SW was examined using a Temkin isotherm model to determine the adsorbent characteristics [35]. The Temkin Plots (q_e vs. C_e) are shown in Fig. 12 for heavy metal ion (Cr, Pb, and Zn) adsorption, and the kinetic constants (K_T & b) were calculated from the plots. At 30°C, the Temkin isotherm model was found to fit with the adsorption process by referring to the R^2 values from Table 4. Also, the fitting process of adsorption with Temkin isotherm studies indicates the binding energies and their uniform distribution. In addition, the high amount of metal ion adsorption indicated the monolayer adsorption process during the SWs and metal ion interactions [36].

Sips isotherm

The constants of the Sips model Q_{max} & K_s were obtained by taking slope and deflection values from the kinetic linear plots of this model (Fig. 13). The values of constants and regression standards are represented in Table 4. The coefficient of regression (R^2) value is lower than 0.95, which indicates the non-fitting process of metal ion adsorption. Based on the heterogeneity factor (n) value, the model describes the nature of fitting, and the value of n lies between 0 to 1. If the n value reaches 1, this Equation reduces to the Langmuir Equation and infers the adsorption process's inhomogeneous nature. Based on the adsorption fitting, the sips model describes the process of adsorption does not follow the multilayer adsorption process with a homogeneous nature.

D-R Adsorption Isotherm

To assess the nature of the adsorbent, the method of adsorption by SW was explored by the D-R isotherm

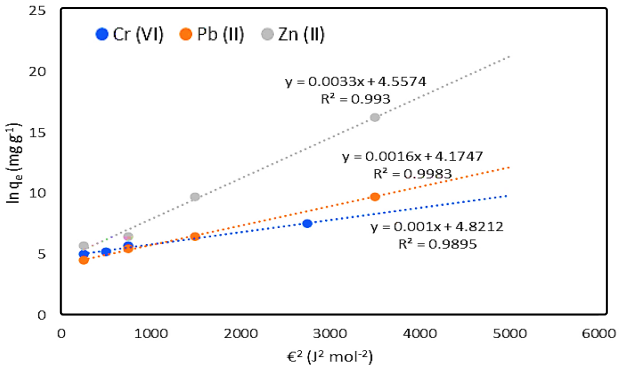

Fig. 14: D – R plot for the adsorption for heavy metals (Cr, Pb and Zn) using SW.

study. The plots of D-R isotherm (ln q_e vs $€^2$) for chromium, lead, and zinc metal ions are shown in Fig. 14, and the constants are presented in Table 4. By fixing a constant temperature of 30°C, the regression coefficient (R^2) values were calculated, and the values were observed to agree ($R^2 > 0.95$) with the adsorption process [37]. The R^2 values calculated by Temkin, D – R and Sips isotherm plots were compared to each other to find the best fit for the isotherm study. The results, Chromium: Temkin > D-R > Sips, Lead Temkin > D-R > Sips and Zinc: Temkin > D-R > Sips, fitted very well with each other. The Temkin isotherm study fitted well with the adsorption process, compared to the D-R & Sips model, based on the obtained R^2 values indicating monolayer adsorption on the SW surface. Nevertheless, the R^2 values were in agreement with Temkin and D-R isotherms, which followed the monolayer & heterogeneous adsorption.

Thermodynamic studies on metal ion adsorption by SW

The removal efficiency of heavy metal ions by SW adsorbent was investigated under different temperature

Table 4: Isotherm constants for metal ion adsorption.

Type of study	Metal ions				
	Parameters	Units	Cr (VI)	Pb (II)	Zn (II)
Temkin	K_T (L/mol)	l/mol	1.27 X 10^7	1.05 X 10^5	1.88 X 10^4
	b x 10^{-6}	Jg/mol	25.6	12.1	23.8
	R^2	-	0.989	0.965	0.956
D-R	X_m x 10^{-3}	(mol/g)	4.15	4.65	3.76
	€	KJ/mol	11.75	10.62	10.31
	R^2	-	0.989	0.950	0.976
Sips	K_S	bar^{-1}	12.8689	6.13959	3.7113
	β_S	mmol/g	1.25346	1.54742	1.6536
	a_S	-	0.47347	0.24345	0.1544
	R^2	-	0.9182	0.9599	0.9991

conditions (15 to 60 °C). Referring to Fig. 15, it was observed that the metal ion adsorption and its efficiency were highly dependent on the temperature. The highest metal ion adsorption by the adsorbent was recorded at 20 °C; beyond that, a sharp decrease in adsorption efficiency was noticed. Due to the reduction of surface activity, the metal ion adsorbent reached the exothermic state [38]. The thermodynamic plots (log Kc vs. 1/T) of the metal ion adsorption process are shown in Fig. 16, and the slope and intercept values (ΔH° & ΔS°) were calculated and presented in Table 5 under different concentrations (25- 150 mg/L) of metal ions. Due to the spontaneous nature of the adsorption process, the negative ΔH° values with negative ΔG° values indicated the exothermic nature of the adsorption process [39]. Also, the ΔS° values suggested increased uncertainty during the metal ion adsorption by SW in aqueous solutions.

Batch desorption study

the ability of the spent adsorbent (SWs) to desorption of metal ions is directly proportional to the desorption process [40]. The batch desorption study was carried out by varying the sulfuric acid concentrations from 0.1 to 0.4 N, and its impact on the recovery of heavy metal ions is represented in Table 6. The maximum amount of recovery of metal ions was determined by increasing the concentration of sulfuric acid. In this work, the total amount of heavy metal ions and their recovery was achieved by adding 0.3 N of H_2SO_4, and thereafter the metal ion recovery attained a constant rate. Further, an increase in the concentration of H_2SO_4 was not found to increase the metal ion recovery from the spent SW. As a result, at 0.3 N of H_2SO_4, the optimal level of desorption of metal ions from waste SW was achieved.

Table 5: Thermodynamic constants of the metal ion adsorption by SW.

Cr ion (Initial Conc.)	ΔH^0 (KJ/mol)	ΔS^0 (J/mol/	ΔG_o (kJ/mol)			
			15°C	30°C	45°C	60°C
25	-83.38	222.52	-15.90	-10.82	-9.24	-8.24
50	-42.73	96.87	-11.31	-8.98	-7.45	-7.32
75	-26.45	61.28	-8.60	-7.45	-6.58	-6.15
100	-19.64	41.29	-6.69	-6.72	-6.19	-5.93
125	-16.82	32.35	-6.24	-6.12	-5.68	-5.28
150	-13.76	24.28	-5.45	-5.84	-5.12	-4.98
Pb ion (Initial Conc.)						
25	-56.24	143.77	-13.30	-11.15	-8.93	-8.13
50	-31.69	72.86	-9.02	-8.80	-7.47	-6.69
75	-26.44	56.98	-8.12	-6.90	-6.64	-5.51
100	-19.89	39.31	-7.62	-6.09	-5.38	-5.20
125	-15.49	21.83	-6.63	-5.44	-4.92	-4.69
150	-11.27	15.98	-5.57	-4.84	-4.52	-4.09
Zn ion (Initial Conc.)						
25	-40.02	99.09	-11.16	-9.29	-8.54	-7.31
50	-25.45	51.27	-9.01	-7.89	-7.02	-6.02
75	-19.92	40.51	-7.69	-6.32	-5.93	-5.29
100	-15.56	31.48	-6.24	-5.89	-5.05	-4.78
125	-13.29	28.92	-5.92	-5.02	-4.58	-4.22
150	-11.92	25.59	-5.01	-4.32	-4.10	-4.00

Table 6: Desorption of metal ions from the spent SW.

Initial concentration (25 mg/L)	Efficiency of metal ion removal (%)	Concentration of H_2SO_4			
		0.10 N	0.20 N	0.30 N	0.40 N
		% Desorption of metal ions			
Cr	99.60	89.26	93.57	93.82	91.31
Pb	89.27	80.93	83.25	83.94	81.84
Zn	82.37	71.73	74.58	75.23	73.83

Furthermore, the SW was recovered and utilised as an adsorbent in subsequent adsorption tests.

Mechanism of metal ion adsorption by green algae

Fig. 17 represents the adsorption mechanism of heavy metal ions using green algae biosorbent and it confirms the process of metal ion uptake by the adsorbent was influenced by external film or intraparticle diffusion. Sometimes, the intraparticle and external film diffusion was happened simultaneously under extraordinary conditions [41]. But in this case the adsorption process

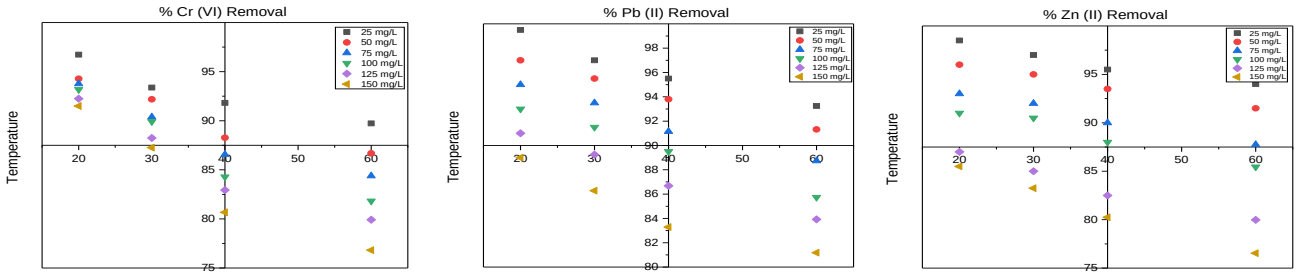

Fig. 15: Impact of temperature of metal ions (Cr, Pb & Zn) adsorption using SW.

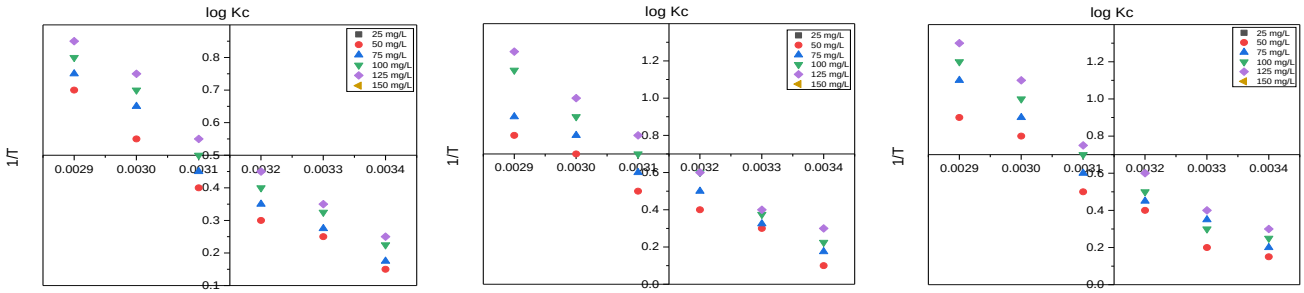

Fig. 16: Thermodynamic plots for the adsorption of metal ions (Cr, Pb & Zn) using SW.

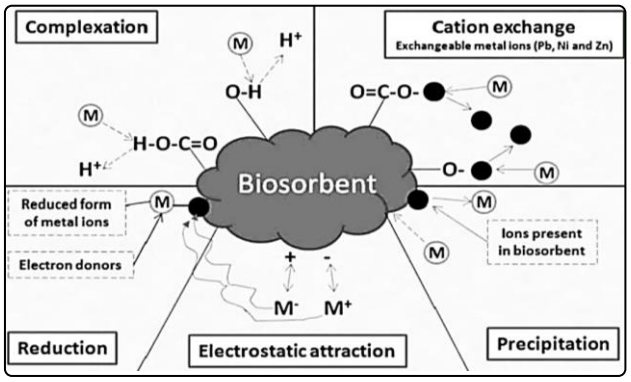

Fig. 17: Mechanism of metal ion adsorption using SW biosorbent

followed three different stages. The first stage represents the metal ion uptake by the adsorbent following external film diffusion and it represents the movement of metal ions to the biochar adsorbent due to the external forces. The second stage represents the heavy metal ions and their pollutants moved into the inner walls of the biosorbent surface due to particle diffusion. The third stage represents the metal ion uptake by the biosorbent was happens due to the deep penetration of metal ions into the adsorbent pores and binding spaces.

CONCLUSIONS

The removal efficiency of Chromium, Lead, and Zinc metal ions present in aqueous solutions was examined using Sargassum Wightii as an adsorbent. At a pH of 2.0, the highest removal efficiency of 99.6 % (Cr)and 88.27% (Pb) and 82.39% (Zn) was achieved by using the batch adsorption study. The ideal condition was found at an adsorbent dose level of 2.0 g/L, a contact period of 60 minutes, an initial adsorbate concentration of 25 mg/L and a temperature of 30°C. The Temkin and D-R isotherm models suited the isotherm investigations well, and the process followed the pseudo-second-order and Boyd kinetic models. As a result, the reported research infers Sargassum Wigtii's capacity to eliminate harmful metal ions from an aqueous medium.

Received: Dec. 23, 2022; Accepted: May. 22, 2023

REFERENCES

[1] Al – Homaidan Ali A., Al – Qahtani Hussein A., Al- Ghanayem Abdullah A., Ameen F., Ibraheem B.M., Potential Use of Green Algae as a Biosorbent for Hexavalent Chromium Removal from Aqueous Solutions, *Saudi Journal of Biological Sciences*., **25(8):** 1733–1738 (2018).

[2] Lucai A.R., Bulgariu D., Christina Popescu M., Bulgariu L., Adsorption of Cu (II) Ions on Adsorbent Materials Obtained from Marine Red Algae Callithamnion Corymbosum sp, *Water*, **12:** 372 (2020).

[3] Mahvi A.H., Balarak D., Bazrafshan E., Remarkable Reusability of Magnetic Fe_3O_4-Graphene Oxide Composite: a Highly Effective Adsorbent for Cr (VI) Ions, *International Journal of Environmental Analytical Chemistry*, **103(15):** 3501-3521 (2021).

[4] Solisio C., Al Arni S., Converti A., Adsorption of Inorganic Mercury from Aqueous Solutions onto Dry Biomass of Chlorella Vulgaris: Kinetic and Isotherm Study, *Environmental Technology*, **40:** 664-672 (2019).

[5] Zunaithur Rahman D., Vijayaraghavan J., Thivya J., A Comprehensive Review on Zinc(II) Sequestration from Wastewater Using Various Natural/Modified Low-Cost Agro-Waste Sorbents, *Biomass Conversion and Biorefinery*, **13:** 5469-5499 (2021).

[6] Dittmann D., Saal L., Zietzschmann F., Mai M., Altmann K., Al-Sabbagh D., Schumann P., Sebastian Ruhl A., Jekel M., Braun U., Characterization of Activated Carbons for Water Treatment Using TGA-FT-IR for Analysis of Oxygen-Containing Functional Groups, *Applied Water Science*, **12:** 203 (2022).

[7] Trikkaliotis D.G., Ainali N.M., Tolkou A.K., Mitropoulos A.C., Lambropoulou D.A., Bikiaris D.N., Kyzas G.Z., Removal of Heavy Metal Ions from Wastewaters by Using Chitosan/Poly (Vinyl Alcohol) Adsorbents: A Review, *Macromol*, **2(3):** 403–425 (2022).

[8] Ouyang D., Zhuo Y., Hu L., Zeng Q., Hu Y., He Z., Research on the Adsorption Behaviour of Heavy Metal Ions by Porous Material Prepared with Silicate Tailings, *Minerals*, **9:** 291 (2019).

[9] Bazrafshan E., Sobhanikia M., Mostafapour F.K., Kamani H., Balarak D., Chromium Biosorption from Aqueous Environments by Mucilaginous Seeds of Cydonia Oblonga: Kinetic and Thermodynamic Studies, *Global Nest Journal*, **19(2):** 269–277 (2017).

[10] Revellame E.D., Lord Fortela D., Sharp W., Hernandez R., Zappi M.E., Adsorption Kinetic Modeling Using Pseudo-First Order and Pseudo-Second order Rate Laws: A Review, *Cleaner Engineering and Technology*, **1:** 100032 (2020).

[11] Erdal Kacan., Optimum BET Surface Areas for Activated Carbon Produced from Textile Sewage Sludges and its Application as Dye Removal, *Journal of Environmental Management*, **166:** 116–123 (2016).

[12] Kajjumba G.W., Yildirim E., Osra F., Aydin S., Kieu Ngan T.T., Emik S., Insights into Nonlinear Adsorption Kinetics and Isotherms of Vanadium Using Magnetised Coal-Polyaniline, *Desalination and Water Treatment*, **172:** 158–166 (2019).

[13] Al-Senani G.M., Al-Fawzan F.F., Adsorption Study of Heavy Metal Ions from Aqueous Solution by Nanoparticle of Wild Herbs, *The Egyptian Journal of Aquatic Research*, **44(3):** 187–194 (2018).

[14] Bullen J.C., Saleesongsom S., Gallagher K., Weiss D.J., A Revised Pseudo-Second-Order Kinetic Model for Adsorption, Sensitive to Changes in Adsorbate and Adsorbent Concentrations, *Langmuir*, **37(10):** 3189-3201 (2021).

[15] Abdulsalam J., Mulopo J., Oboirien B., Bada S., Falcon R., Experimental Evaluation of Activated Carbon Derived from South Africa Discard Coal for Natural Gas Storage, *Inter. J. Co. Sci. Tech.*, **6:** 459–477 (2019).

[16] Yang J., Hou B., Wang J., Tian B., Bi J., Wang N., Xin Li., Huang X., Nanomaterials for the Removal of Heavy Metals from Wastewater, *Nanomaterials*, **9:** 424 (2018).

[17] Dulla J.B., Tamana M.R., Boddu S., Pulipati K., Srirama K., Biosorption of Copper (II) onto Spent Biomass of Gelidiella Acerosa (Brown Marine Algae): Optimization and Kinetic Studies, *Applied Water Science*, **10:** 56 (2020).

[18] Saleem J., Shahid U.B., Hijab M., Mackey H., McKay G., Production and Applications of Activated Carbons as Adsorbents from Olive Stones, *Biomass Conversion and Biorefinery*, **9:** 775–802 (2019).

[19] Kaparapu J., Prasad M.K., Equilibrium, Kinetics and Thermodynamic Studies of Cadmium (II) Biosorption on Nannochloropsis Oculate, Applied Water Science, **8:** 179 (2018).

[20] Kipigroch K., The Use of Algae in the Process of Heavy Metal Ions Removal from Wastewater, *Desalination and Water Treatment*, **134:** 289 – 295 (2018).

[21] Kumar M., Singh A.K., Sikardhar M., Biosorption of Hg (II) from Aqueous Solution Using Algal Biomass: Kinetics and Isotherm Studies, *Heliyon*, **6(1):** e03321 (2020).

[22] Manjuladevi M., Anitha R., Manonmani S., Kinetic Study on Adsorption of Cr (VI), Ni (II), Cd (II) and Pb (II) Ions from Aqueous Solutions Using Activated Carbon Prepared from Cucumis Melo Peel, *Applied Water Science*, **8:** 36 (2018).

[23] Feszterová M., Porubcová L., Tirpáková A., The Monitoring of Selected Heavy Metals Content and Bioavailability in the Soil-Plant System and Its Impact on Sustainability in Agribusiness Food Chains, *Sustainability*, **13:** 7021 (2021).

[24] Momina., Rafatullah M., Ismail M., Ahmed A., Optimization Study for the Desorption of Methylene Blue Dye from Clay Based Adsorbent Coating, *Water*, **11:** 1304 (2019).

[25] Adnan M., Xiao B., Xiao P., Zhao P., Li R., Bibi S., Research Progress on Heavy Metals Pollution in the Soil of Smelting Sites in China, *Toxics*, **10:** 231 (2022).

[26] Ghayedi N., Borazjani J.M., Jafari D., Biosorption of Arsenic Ions from the Aqueous Solutions Using Chlorella Vulgaris Micro Algae, *Desalination and Water Treatment*, **165:** 188 – 196 (2019).

[27] Al-Harby N.F., Albahly E.F., Mohamed N.A., Kinetics, Isotherm and Thermodynamic Studies for Efficient Adsorption of Congo Red Dye from Aqueous Solution onto Novel Cyanoguanidine-Modified Chitosan Adsorbent, *Polymers*, **13:** 4446 (2021).

[28] Lawtae P., Tangsathitkulchai C., The Use of High Surface Area Mesoporous-Activated Carbon from Longan Seed Biomass for Increasing Capacity and Kinetics of Methylene Blue Adsorption from Aqueous Solution, *Molecules*, **26:** 6521 (2021).

[29] Saavedra R., Muñoz R., Taboada M.E., Vega M., Bolado S., Comparative Uptake Study of Arsenic, Boron, Copper, Manganese and Zinc from Water by Different Green Microalgae, *Bioresource Technology*, **263:** 49–57 (2018).

[30] Rico I.L.R., Carrazana R.J.C., Karna N.K., Modeling the Mass Transfer in Biosorption of Cr (VI) y Ni (II) by Natural Sugarcane Bagasse, *Applied Water Science*, **8:** 55 (2018).

[31] Agarwal S., Tyagi I., Gupta V.K., Dehghani M.H., Jaafari J., Balarak D., Asiff M., Rapid Removal of Noxious Nickel (II) Using Novel γ-Alumina Nanoparticles and Multiwalled Carbon Nanotubes: Kinetic and Isotherm Studies, *Journal of Molecular Liquids*, **224:** 618-623 (2016).

[32] Umeh T.C., Nduka J.K., Akpomie K.G., Kinetics and Isotherm Modeling of Pb (II) and Cd (II) Sequestration from Polluted Water onto Tropical Ultisol Obtained from Enugu Nigeria, *Applied Water Science*, **11:** 65 (2021).

[33] Yogeshwaran V., Priya A.K., Experimental Studies on the Removal of Heavy Metal Ion Concentration Using Sugarcane Bagasse in Batch Adsorption Process, *Desalination and Water Treatment*, **224:** 256–272 (2021).

[34] Madjene F., Chergui A., Trari M., Biosorption of Ni (II) by Fig Male: Optimization and Modeling Using a Full Factorial Design, *Water Environment Research*, **88(6):** 540–547 (2016).

[35] Madjene F., Danane F., Chergui A., Trari M., Biosorption of Cr (VI) Ions onto Walnut Flowers: Application of Isotherm Models, *Iranian Journal of Chemistry and Chemical Engineering (IJCCE)*, **41(12):** 4039-4047 (2022).

[36] Firat Baran M., Zahir Duz M., Removal of Cadmium (II) in the Aqueous Solutions by Biosorption of Bacillus Licheniformis Isolated from Soil in the Area of Tigris River, *Inter. J. Envir. Analytical Chem.*, **101(4):** 533–548 (2019).

[37] Firat Baran M., Zahir Duz M., Biosorption of Pb^{2+} from Aqueous Solutions by Bacillus Licheniformis Isolated from Tigris River with a Comparative Study, *International Journal of Latest Engineering and Management Research*, **4(5):** 108–121 (2019).

[38] Firat Baran M., Zahir Duz M., Uzan S., Dolak I., Celik S., Kilinc E., Removal of Hg (II) from Aqueous Solution by Bacillus Subtilis ATCC 6051(B1), *Journal of Bioprocessing & Biotechniques*, **8(4):** 1000329 (2018).

[39] Malima N., Owonubi S.J., Lugwisha E.H., Mwakaboko A.S., Thermodynamic, Isothermal and Kinetic Studies of Heavy Metals Adsorption by Chemically Modified Tanzanian Malangali Kaolin Clay. *International Journal of Environmental Science and Technology*, **18(10):** 1-16 (2021).

[40] Yahya M.D., Aliyu A.S., Obayomi K.S., Olugbenga A.G., Abdullahi U.B., Column Adsorption Study for the Removal of Chromium and Manganese from Electroplating Wastewater Using Cashew Nutshell Adsorbent, *Chemical engineering*, **7:** 1748470 (2020).

[41] Yaseen D.A., Scholz M., Textile Dye Wastewater Characteristics and Constituents of Synthetic Effluents: A Critical Review, *International Journal of Environmental Science and Technology*, **16:** 1193–1226 (2018).